



1 **Estimating Beam Pointing of Vertically Pointing Cloud Radars Using**  
2 **Radiosonde Measurements**

3 Min Deng<sup>1</sup>, Scott E. Giangrande<sup>1</sup>, Adam K. Theisen<sup>2</sup>, Karen Johnson<sup>1</sup>, Iosif A.  
4 Lindenmaier<sup>3</sup>, Timothy G. Wendler<sup>3</sup>, Jennifer Comstock<sup>3</sup>, Marquette Rocque<sup>3</sup>, Zeen  
5 Zhu<sup>1</sup>, and Alyssa Matthews<sup>3</sup>.

6  
7 <sup>1</sup>Brookhaven National Laboratory,

8 <sup>2</sup>Argonne National Laboratory,

9 <sup>3</sup>Pacific Northwest National Laboratory

10

11 *Correspondence to:* Min Deng (mdeng@bnl.gov)

12

13

14

15

16

17

18

19

20

21

22

23

24

25

26

27

28

29

30

31

32

33

34

35

36

37

38

39

40

41



42 **Abstract**

43 Accurate beam pointing is essential for vertically pointing cloud radars, as even small  
44 tilting off zenith introduces projections of horizontal wind into Doppler velocity  
45 measurements. These effects can bias the interpretation of vertical air motion and  
46 hydrometeor fall speeds, leading to systematic errors in cloud and precipitation  
47 retrievals.

48 We present a method to estimate and validate radar beam pointing angle using  
49 collocated radiosonde observations. When the radar beam is tilted, the observed  
50 Doppler velocity exhibits a cosine dependence on wind direction due to projection of  
51 horizontal wind onto the beam, with an amplitude proportional to wind speed. By  
52 normalizing Doppler velocity with horizontal wind speed, this geometric dependence  
53 can be isolated, enabling quantitative retrieval of off-zenith beam pointing estimation.

54 The method is applied to the Ka-band ARM Zenith Radar (KAZR) and the Marine W-  
55 band ARM Cloud Radar (MWACR) during the Cloud and Precipitation Experiment at  
56 Kennaook (CAPE-k). Results show a clear wind-direction dependence consistent with  
57 small but measurable beam pointing offsets. Differences in Doppler velocity between  
58 KAZR and MWACR further reduce the influence of hydrometeor fall velocity and  
59 vertical air motion, providing an independent constraint on relative pointing errors.  
60 Application to KAZR observations at ARM fixed sites and recent field campaigns  
61 further demonstrates that the method is robust across a range of atmospheric  
62 conditions. This approach provides a practical and scalable tool for evaluating radar  
63 beam pointing using routinely available radiosonde data, with direct implications for  
64 improving the accuracy of ARM cloud and precipitation products.

65 **Short Summary**

66 Cloud radars are used to measure air motion, clouds, and precipitation, but even very  
67 small pointing errors can affect their accuracy. We developed a method to detect these  
68 pointing offsets using routine weather balloon observations. The method was tested  
69 on several radar systems deployed in different environments and successfully  
70 identified small but important pointing biases. This approach provides a practical way  
71 to improve the quality and long-term consistency of cloud and precipitation  
72 measurements used in weather and climate research.



73 **1. Introduction**

74 Vertically pointing cloud radars have become essential tools for observing cloud  
75 structure, microphysics, and atmospheric dynamics at high temporal and spatial  
76 resolution. Measurements of radar reflectivity and Doppler velocity from these systems  
77 provide key information for studies of cloud processes, precipitation formation, and  
78 vertical air motion. Doppler velocity observed by vertically pointing radars is commonly  
79 interpreted as the sum of hydrometeor fall velocity and vertical air motion, forming the  
80 basis for numerous retrieval techniques for in-cloud vertical velocity, turbulence, and  
81 microphysical properties. These measurements have been widely used to investigate  
82 boundary layer clouds, mixed-phase and ice cloud processes, and precipitation  
83 dynamics (e.g., Kollias et al., 1999; Deng et al. 2006, 2008, Shupe et al., 2008; Kollias  
84 et al., 2014).

85 The United States Department of Energy (DOE) Atmospheric Radiation Measurement  
86 user facility (ARM) has continuously deployed vertically pointing cloud radars at fixed  
87 and mobile observatories since 1996 (Kollias et al., 2016). Initially, the Ka-band  
88 Millimeter Cloud Radar (MMCR) was deployed, then in 2011, ARM transitioned to the  
89 Ka-band ARM Zenith Radar (KAZR) and the Marine W-band ARM Cloud Radar  
90 (MWACR). Both KAZR and MWACR were recently deployed to kennaook Tasmania  
91 to support the Cloud and Precipitation Experiment at kennaook (CAPE-k).

92 A fundamental challenge in Doppler radar analysis is the separation of vertical air  
93 motion from hydrometeor fall velocity. Techniques based on Doppler spectra and  
94 Doppler moments, including spectral decomposition and identification of Mie  
95 scattering signatures, have been developed to isolate the air motion component in  
96 cloud and precipitation systems (e.g., Lhermitte, 1988; Kollias et al., 2002; Kollias et  
97 al., 2007; Shupe et al., 2008; Deng and Mace, 2006 and 2008; Kalesse and Kollias,  
98 2013). These studies demonstrate that millimeter-wavelength Doppler spectra and  
99 moments contain detailed information on particle fall velocities, turbulence broadening,  
100 and vertical air motion, although retrieval accuracy depends on assumptions regarding  
101 particle size distributions and scattering regimes. Complementary observations, such  
102 as lidar identification of liquid cloud layers and thermodynamic constraints from  
103 radiosonde measurements, can provide additional context for interpreting Doppler  
104 spectra and reducing uncertainty in vertical velocity estimates (e.g., Shupe et al., 2008;



105 Kollias et al., 2014; Zhu et al., 2021). Together, these studies highlight the capability  
106 of vertically pointing cloud radars to resolve fine-scale atmospheric motions in clouds.

107 A fundamental assumption underlying these applications is that the radar beam is  
108 accurately aligned with the local vertical. However, even small deviations from zenith  
109 can introduce systematic biases in Doppler velocity through projection of horizontal  
110 wind onto the radar beam. For a perfectly vertical beam, horizontal wind does not  
111 contribute to the measured Doppler velocity. In contrast, a small zenith angle offset  
112 produces a wind-direction-dependent Doppler signal, which can introduce bias in  
113 retrieved vertical air motion and turbulence estimates. This sensitivity is particularly  
114 important for millimeter-wavelength cloud radars such as the KAZR and MWACR,  
115 which are designed to detect small velocity perturbations associated with weak cloud  
116 motions and boundary layer turbulence. As a result, even sub-degree pointing  
117 uncertainties can lead to measurable biases in Doppler velocity and derived  
118 geophysical products.

119 Despite the importance of accurate beam alignment, relatively few studies have  
120 directly quantified beam pointing errors for vertically pointing cloud radars. Existing  
121 approaches have primarily relied on engineering alignment procedures, statistical  
122 characteristics of Doppler velocity, or comparison with independent wind  
123 measurements. The systematic evaluation of the Doppler velocity–wind direction  
124 relationship for beam pointing estimation remains limited. In particular, the sensitivity  
125 of the approach to atmospheric variability, wind speed magnitude, and instrument  
126 characteristics has not been extensively assessed across different radar systems and  
127 observational environments. In addition, the consistency of pointing estimates derived  
128 from multiple co-located cloud radars operating at different frequencies has not been  
129 thoroughly examined. Understanding these uncertainties is important because  
130 pointing biases can propagate directly into retrievals of vertical air motion and cloud  
131 microphysical properties.

132 Radiosonde observations provide a particularly valuable reference because they offer  
133 high-resolution vertical profiles of horizontal wind speed and direction that are  
134 independent of radar calibration assumptions. In this study, we develop and apply a  
135 monitoring method to estimate and validate the beam pointing of vertically pointing  
136 cloud radars using collocated radiosonde wind measurements. The method exploits



137 the cosine dependence of Doppler velocity on wind direction to retrieve off-zenith  
138 pointing angle and to quantify their impact on Doppler velocity observations. The  
139 approach is applied to observations from the KAZR and the MWACR collected during  
140 multiple ARM field campaigns and fixed sites, enabling cross-instrument comparison  
141 and evaluation of relative pointing differences. The results provide new insight into the  
142 magnitude and variability of beam mispointing and demonstrate a practical framework  
143 for monitoring the vertically pointing radar measurements and evaluating the related  
144 retrieval products.

145

## 146 **2. Data Description**

### 147 2.1 Cloud radar observations

148 Observations from the CAPE-k KAZR (~35 GHz) and the MWACR (~94 GHz) are used  
149 in this study. KAZR and MWACR were sited to each other within 200 meters. KAZR  
150 has an antenna diameter of 1.8 m and a one-way half-power beam width (HPBW) of  
151 approximately 0.3°, while the MWACR operates with a smaller antenna diameter of  
152 about 0.5–0.6 m and a broader HPBW of approximately 0.8°.

153 They provide high-sensitivity measurements of cloud and precipitation properties  
154 (Kollias et al. 2007; Widener et al. 2012; Bharadwaj et al. 2013). They are designed  
155 primarily for vertically pointing observations to provide continuous time–height retrieval  
156 products of cloud properties and air motion (Kollias et al. 2014; Isom et al. 2013).

157 Radar reflectivity ( $Z_e$ ) and Doppler velocity ( $V_d$ ) are derived from Doppler spectra  
158 obtained by the cloud radar signal processor. Radar moments are computed from the  
159 Doppler spectrum following clutter filtering and noise removal (Doviak and Zrníć 1993;  
160 Kollias et al. 2002). Radar reflectivity factor is proportional to the sixth moment of the  
161 particle size distribution, while Doppler velocity is calculated as the power-weighted  
162 mean radial velocity of scatterers within the radar sampling volume. Under the  
163 assumption of vertical beam pointing, Doppler velocity primarily represents the  
164 combined contribution of hydrometeor fall velocity and vertical air motion (Kollias et al.  
165 2001; Shupe et al. 2008).



166 In this study, vertically pointing observations from KAZR and MWACR are analyzed to  
167 assess the consistency of Doppler velocity measurements and to diagnose potential  
168 beam mispointing of each instrument. The use of two independent cloud radars at the  
169 same site also provides an opportunity to do cross comparison for evaluating  
170 systematic differences in Doppler velocity between them.

## 171 2.2 Radiosonde observations

172 Radiosonde observations provide independent measurements of atmospheric state  
173 variables, including temperature, pressure, horizontal wind speed, and wind direction.  
174 Wind profiles from radiosondes are derived from GPS tracking of balloon position,  
175 providing estimates of the horizontal wind vector as a function of height (Dirksen et al.  
176 2014; Nash et al. 2011, Keeler 2025). These measurements serve as an external  
177 reference for evaluating the relationship between Doppler velocity and horizontal wind  
178 direction observed by vertically pointing cloud radars. Typical uncertainties in  
179 radiosonde wind measurements are approximately  $0.5\text{--}1.0\text{ m s}^{-1}$  for wind speed and  
180  $5\text{--}10^\circ$  for wind direction, depending on atmospheric conditions and instrument type  
181 (Nash et al. 2011; Dirksen et al. 2014).

182 A known limitation in radar–radiosonde comparisons is the horizontal displacement of  
183 the radiosonde during ascent. As the balloon ascends through the atmosphere, it drifts  
184 with the ambient wind, resulting in spatial separation between the radiosonde  
185 measurement location and the radar sampling volume. Previous studies have shown  
186 that radiosonde drift distances typically range from 5 to 30 km by the time the balloon  
187 reaches 10 km altitude, depending on wind conditions (Seidel et al. 2011; Nash et al.  
188 2011). This spatial displacement introduces uncertainty when comparing radiosonde  
189 winds with vertically pointing radar measurements, particularly in environments with  
190 strong horizontal wind shear or spatial variability in cloud structure.

191 Despite this limitation, radiosonde wind measurements have been widely used as a  
192 reference for validating radar-derived wind and Doppler velocity observations because  
193 they provide reliable estimates of the large-scale wind field (May and Rajopadhyaya  
194 1999; Kollias et al. 2007). In this study, the horizontal wind speed ( $U$ ) and wind  
195 direction ( $\phi$ ) derived from radiosonde observations are combined with radar Doppler  
196 velocity measurements to evaluate the contribution of horizontal wind to the observed



197 Doppler velocity. The comparison assumes that horizontal wind variability over the  
198 radiosonde drift distance is relatively small compared to the wind direction dependent  
199 Doppler velocity signal associated with radar beam mispointing.

200

201 2.3 Case study of the Vd contribution from horizontal wind

202

203 Figure 1 shows time–height cross sections of radar reflectivity ( $Z_e$ ) and Doppler  
204 velocity ( $V_d$ ) from KAZR and MWACR at the CAPE-k site on 6 September 2024. Both  
205 radars observe an extensive cloud layer between approximately 5–8 km, indicating  
206 consistent detection of the cloud structure. Within this layer, KAZR reflectivity is  
207 comparably larger than MWACR reflectivity, which may reflect calibration differences  
208 or frequency-dependent scattering effects between the Ka-band and W-band radar  
209 measurements.

210 The Doppler velocity fields show a systematic difference between the two radars.  
211 MWACR Doppler velocities are generally weakly downward, with magnitudes around  
212 0–0.5  $\text{m s}^{-1}$ , consistent with expected fall speeds of small ice particles in stratiform  
213 cloud conditions. In contrast, KAZR Doppler velocities increase from near 0  $\text{m s}^{-1}$  at  
214 cloud base at 5 km to values approaching 2  $\text{m s}^{-1}$  upward toward cloud top at about 8  
215 km, which is unlikely to result from persistent upward air motion over such an extended  
216 layer. The Doppler velocity difference between KAZR and MWACR shows a consistent  
217 positive bias in KAZR measurements, suggesting a possible contribution from beam  
218 pointing offsets through projection of horizontal wind onto a slightly tilted KAZR beam.

219 Figure 2 shows the schematic illustration of the geometric relationship between  $V_d$ ,  
220 horizontal wind ( $U$ ), particle fall velocity ( $V_f$ ), and vertical air motion ( $W$ ). When the  
221 radar beam is vertically pointing, the measured  $V_d$  is a summation of  $V_f$  and  $W$ . When  
222 the radar beam deviates from the vertical direction, the measured  $V_d$  has three main  
223 components from the projection of  $U$ ,  $V_f$ , and  $W$  as in following equation:

224

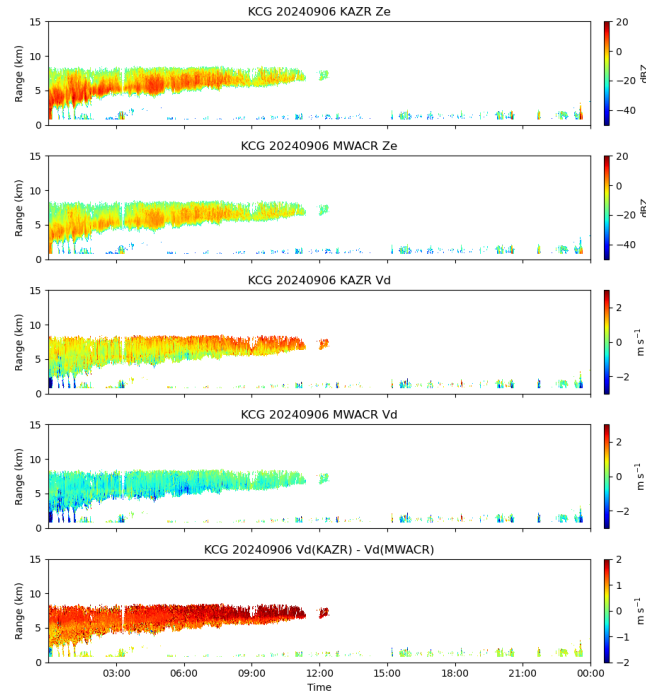


Figure 1. Time–height cross sections of radar reflectivity ( $Z_e$ ) and Doppler velocity ( $V_d$ ) observed by KAZR and MWACR at the CAPE-k site (KCG) on 6 September 2024. Panels show (a) KAZR reflectivity, (b) MWACR reflectivity, (c) KAZR Doppler velocity, (d) MWACR Doppler velocity, and (e) Doppler velocity difference  $V_d(\text{KAZR}) - V_d(\text{MWACR})$ .

225

226

$$v_{d,ka} \approx U \cos(\phi - \phi_{0,ka}) \cos(\theta_{0,ka}) + w \sin(\theta_{0,ka}) - v_{f,ka} \sin(\theta_{0,ka}) + C_{ka}, \quad (1)$$

$$v_{d,w} \approx U \cos(\phi - \phi_{0,w}) \cos(\theta_{0,w}) + w \sin(\theta_{0,w}) - v_{f,w} \sin(\theta_{0,w}) + C_w, \quad (2)$$

227

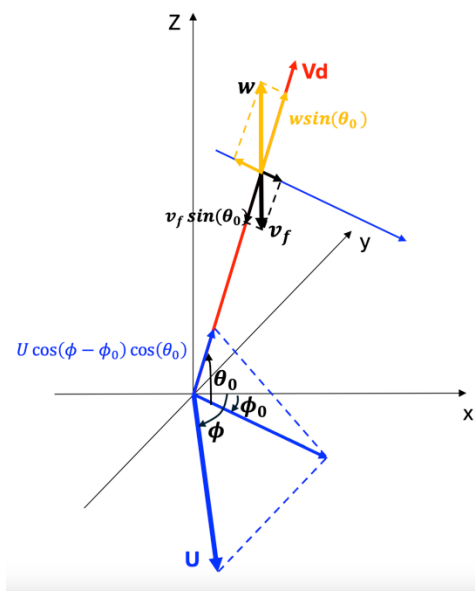


Figure 2. Schematic illustration of the geometric relationship between Doppler velocity ( $V_d$ ), horizontal wind ( $U$ ), particle fall velocity ( $V_f$ ), and vertical air motion ( $w$ ). The radar beam pointing is defined by zenith angle  $\theta_0$  and azimuth angle  $\phi_0$ . The horizontal wind direction is denoted by  $\phi$ . The projection of  $U$ ,  $V_f$ , and  $w$  onto the radar beam contributes to Doppler velocity when the radar beam deviates from the vertical direction.

228

229

230 The radar beam pointing is defined by zenith angle  $\theta_0$  and azimuth angle  $\phi_0$ . In this  
 231 study, the horizontal wind direction  $\phi$  is defined differently from current radiosonde  
 232 convention. It is defined using the vector direction convention, measured clockwise  
 233 from north as the direction toward which the wind flows rather than the direction from  
 234 which it originates, such that  $0^\circ$  indicates northward flow and  $180^\circ$  indicates southward  
 235 flow. The projection of  $U$ ,  $V_f$ , and  $W$  onto the radar beam contributes to Doppler  
 236 velocity when the radar beam deviates from the vertical direction. The  $C_{ka}$  and  $C_w$  are  
 237 the corresponding offsets for KAZR and MWACR, which should be close to zero.

238

239



### 240 **3. Beam Pointing Estimation Method**

#### 241 3.1 Sensitivity of Doppler Velocity to Horizontal Wind and Beam Pointing Angle

242 The contribution of horizontal wind to Doppler velocity increases with both horizontal  
243 wind speed and radar beam off-zenith angle. To illustrate this sensitivity, Doppler  
244 velocity was simulated as a function of wind direction for different horizontal wind  
245 speeds and radar zenith pointing angles, assuming zero particle fall velocity and zero  
246 vertical air motion in order to isolate the contribution of horizontal wind. The azimuth  
247 angle of the radar beam is assumed to be constant at  $135^\circ$ .

248 The results are shown in Figure 3. When the radar beam is perfectly vertical ( $\theta_0 = 90^\circ$ ),  
249 Doppler velocity shows no dependence on horizontal wind speed or wind direction  
250 because the horizontal wind vector is perpendicular to the radar beam. When the radar  
251 beam deviates slightly from vertical pointing, Doppler velocity exhibits a cosine  
252 dependence on wind direction, with maximum magnitude occurring when the  
253 horizontal wind direction is aligned with the radar azimuth angle.

254 For a small pointing offset of  $0.5^\circ$  ( $\theta_0 = 89.5^\circ$ ), the contribution of horizontal wind  
255 produces a weak but detectable Doppler velocity signal. For example, when horizontal  
256 wind speed is  $10 \text{ m s}^{-1}$ , the resulting Doppler velocity magnitude is approximately  $0.05$   
257  $\text{m s}^{-1}$ . For stronger winds of  $40 \text{ m s}^{-1}$ , which are commonly observed in upper-level jet  
258 conditions, the maximum Doppler velocity contribution increases to approximately  $0.3$   
259  $\text{m s}^{-1}$ .

260 As the off-zenith angle increases, the magnitude of the wind-induced Doppler velocity  
261 increases approximately proportionally to  $\cos(\theta_0)$ . Increasing the beam offset from  $0.5^\circ$   
262 to  $1^\circ$  approximately doubles the amplitude of the wind-induced Doppler velocity signal,  
263 while increasing the offset to  $2^\circ$  produces an approximately fourfold increase relative  
264 to the  $0.5^\circ$  case. This strong sensitivity to small pointing offsets demonstrates that the  
265 wind-direction dependence of Doppler velocity provides an effective method for  
266 estimating and validating radar beam pointing.

267

268



269

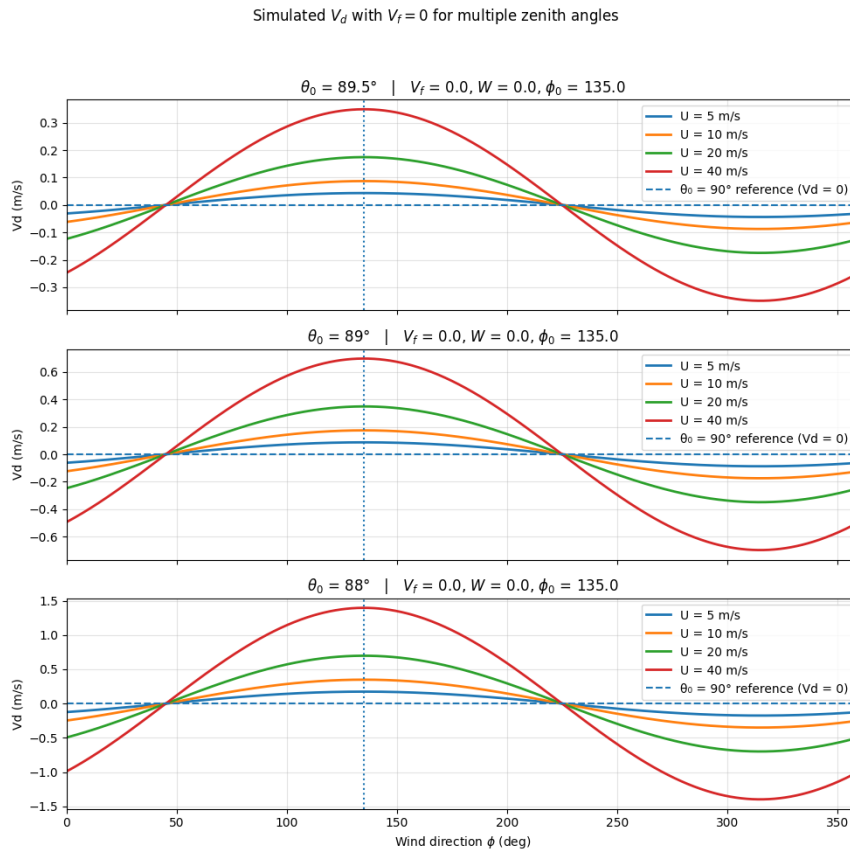


Figure 3 Simulated Doppler velocity ( $V_d$ ) as a function of wind direction for different horizontal wind speeds ( $U$ ) and radar zenith pointing angles ( $\theta_0$ ), illustrating the dependence of  $V_d$  on beam mispointing, assuming zero fall velocity and air motion. a)  $\theta_0 = 89.5^\circ$  b)  $\theta_0 = 89^\circ$  and c)  $\theta_0 = 88^\circ$

270

### 271 3.2 Normalization of Doppler Velocity by Horizontal Wind Speed

272 Equation (1) and Figure 3 show that the contribution of horizontal wind to Doppler  
273 velocity depends on both wind speed and radar beam pointing geometry. Because  
274 horizontal wind speed varies with height and time, direct comparison of Doppler  
275 velocity between radar and radiosonde measurement can be influenced by variability  
276 in wind magnitude. To isolate the geometric contribution of beam pointing to Doppler



277 velocity, the observed Doppler velocity is normalized by horizontal wind speed  
278 obtained from radiosonde measurements.

279 Dividing Eq. (1) by horizontal wind speed  $U$  yields

$$280 \quad \frac{V_d}{U} \approx \cos(\phi - \phi_0) \cos(\theta_0) + \frac{W - V_f}{U} \sin(\theta_0) + \frac{C_{ka}}{U}. \quad (3)$$

281

282 For sufficiently strong horizontal wind speeds, the second and third terms become  
283 small compared to the first term and less of wind direction dependence, especially in  
284 upper-level ice clouds where particle fall velocities are small and vertical air motion is  
285 weak relative to synoptic-scale horizontal wind. Under these conditions, the  
286 normalized Doppler velocity can be approximated as

$$288 \quad \frac{V_d}{U} \approx \cos(\phi - \phi_0) \cos(\theta_0) + C \quad (4)$$

287

289 where  $C$  represents a small constant offset that accounts for the combined contribution  
290 of mean particle fall velocity, mean vertical air motion, and potential calibration bias.

291 This normalization removes the dependence of Doppler velocity magnitude on wind  
292 speed and highlights the cosine dependence on wind direction. As a result, the  
293 normalized Doppler velocity primarily reflects radar beam pointing geometry rather  
294 than atmospheric variability in wind magnitude. Because both KAZR and MWACR  
295 observe the same horizontal wind field, the ratio  $V_d/U$  provides a consistent  
296 framework for comparing beam pointing characteristics between the two radars. The  
297 amplitude of the cosine relationship is proportional to  $\cos(\theta_0)$ , while the phase shift  
298 provides an estimate of the azimuth pointing offset  $\phi_0$ . In addition to the cosine  
299 dependence of  $V_d/U$  associated with off-vertical pointing, atmospheric vertical air  
300 motion and hydrometeor fall velocity contribute additional variability that can introduce  
301 scatter or bias in the expected relationship.

302

303 3.3 Wind dependence of  $V_d$  using Radiosonde Observations



304 To evaluate radar beam pointing using the relationship between Doppler velocity and  
305 horizontal wind, Doppler velocity profiles are compared with collocated radiosonde  
306 wind measurements. For each radiosonde launch, radar Doppler velocity profiles ( $V_d$ )  
307 are averaged within a time window centered on the radiosonde launch time (typically  
308 from  $\pm 30$  to  $\pm 150$  minutes). The temporal averaging reduces variability associated with  
309 turbulence and short-term cloud evolution while maintaining consistency with the  
310 large-scale wind profile measured by the radiosonde.

311 Radiosonde temperature profiles are used to identify atmospheric layers above the  
312 melting level in order to minimize the contribution of precipitation fall velocity. Above  
313 the melting layer, ice-phase particles generally exhibit smaller fall velocities and  
314 reduced variability, making these regions more suitable for isolating the horizontal  
315 wind contribution to Doppler velocity.

316 The averaged Doppler velocity profiles are then examined together with radiosonde  
317 wind speed and wind direction profiles. According to Eq. (1), when the radar beam  
318 deviates slightly from vertical pointing, Doppler velocity exhibits a dependence on  
319 horizontal wind speed and wind direction through the geometric projection of the wind  
320 vector onto the radar beam. The normalized quantity  $V_d/U$  is therefore expected to  
321 follow a cosine dependence on wind direction.

322 Figure 4 shows an example of this processing procedure for the case in Figure 1. In  
323 this case, the wind direction is relatively uniform between approximately surface and  
324 15 km altitude, with winds primarily from the northwest. Wind speed increases  
325 substantially with height, from approximately  $10 \text{ m s}^{-1}$  near surface to nearly  $90 \text{ m s}^{-1}$   
326 near 11 km altitude, consistent with the presence of strong upper-level flow. KAZR  
327 measures two layers of clouds, and the upper layer is our focus here. The Doppler  
328 velocity measured by KAZR exhibits a corresponding increase with height, increasing  
329 from approximately  $0.5 \text{ m s}^{-1}$  near 6 km to about  $2 \text{ m s}^{-1}$  near 8 km. In contrast,  
330 MWACR Doppler velocity exhibits weaker vertical variation, with general downward  
331 motion ranging from 0 to  $0.5 \text{ m s}^{-1}$ .

332 Because the contribution of horizontal wind to Doppler velocity depends primarily on  
333 wind direction rather than altitude, observations from multiple heights within ice cloud  
334 layers can be combined to improve statistical robustness. In individual radiosonde



335 cases, wind direction may not vary sufficiently with height to clearly reveal the cosine  
 336 dependence predicted by Eq. (2). Therefore, observations from multiple radiosonde  
 337 launches throughout the field campaign are combined to obtain a broad sampling of  
 338 wind directions. This aggregation allows identification of the expected cosine  
 339 dependence of normalized Doppler velocity on wind direction and enables estimation  
 340 of radar beam pointing offsets.

KCG launch 2024-09-06 11:30:00 | window 150min

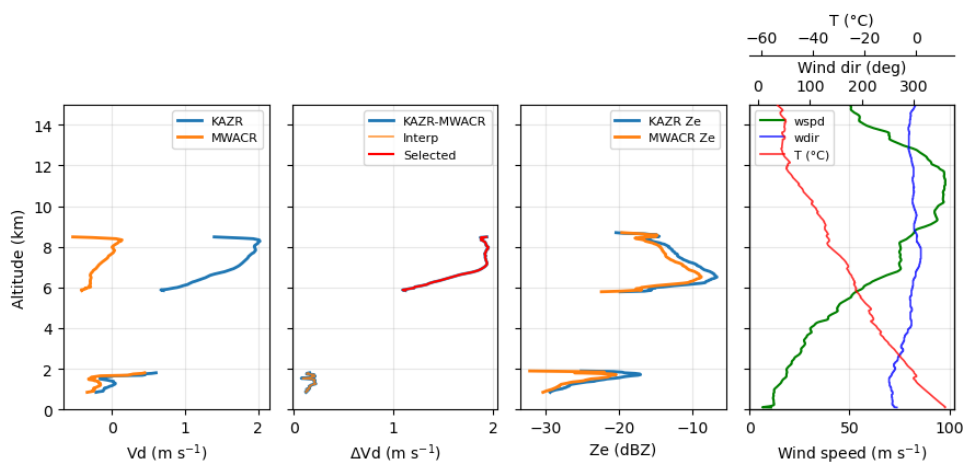


Figure 4 Profiles of KCG KAZR and MWACR Doppler velocity ( $V_d$ ) averaged over a time window centered on the radiosonde launch, together with collocated radiosonde profiles of temperature, wind speed, and wind direction.

341

342

#### 343 4. Method Application and Results

##### 344 4.1 KAZR Observations from the CAPE-k

345 The CAPE-k campaign was deployed from April 15, 2024, to October 15, 2025. The  
 346 dominant wind in cloud from radiosonde measurement in Figure 5a is in 50 to 150  
 347 degrees, which are south-westerly, westerly to north-westerly wind. The  
 348 corresponding Doppler velocity as a function of wind direction Figure 5b shows a  
 349 baseline  $V_d$  at approximately  $-0.8 \text{ m s}^{-1}$ , consistent with typical fall velocities of ice  
 350 particles. Superimposed on this baseline  $V_d$ , a wind-direction-dependent modulation



351 is evident, with maximum positive Doppler velocity at  $1.5 \text{ m s}^{-1}$ , occurring near a wind  
352 direction of approximately  $140^\circ$ , approximate in the radar azimuth angle.

353 The Doppler velocity exhibits substantial variability, especially around 50-150 degree,  
354 due to the combined influence of hydrometeor fall velocity, vertical air motion, and  
355 projection of horizontal wind onto a slightly tilted radar beam as shown in Fig. 5a. The  
356 magnitude of the Doppler velocity variation reaches values close to  $1.5 \text{ m s}^{-1}$ ,  
357 comparable to the simulated wind-projection component shown in Fig. 3c.

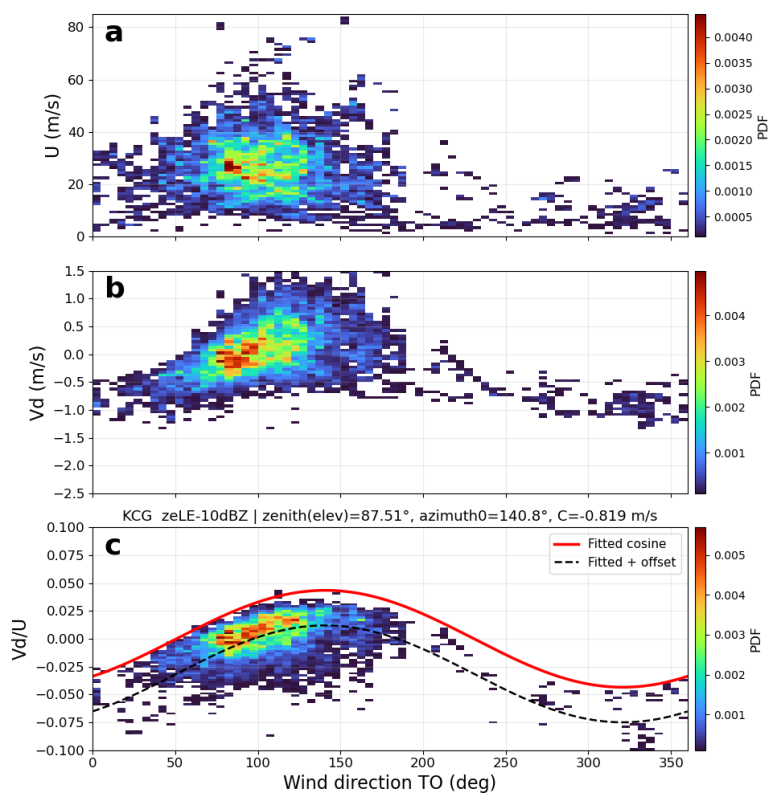


Figure 5. KAZR pointing validation at CAPE-k. (a) Horizontal wind speed (U), (b) Doppler velocity (Vd), and (c) normalized Doppler velocity (Vd/U) as functions of wind direction toward the angle, rather than from the angle as in radar coordinate. In panel (c), cosine fits to Vd/U are shown with and without a constant offset; the offset ( $-0.819 \text{ m s}^{-1}$ ) represents the combined contribution of mean particle fall velocity and vertical air motion.



358 Figure 5c shows the normalized Doppler velocity ( $V_d/U$ ) as a function of wind direction.  
359 After normalization by horizontal wind speed, the dependence of Doppler velocity on  
360 wind direction becomes more clearly defined. The normalized observations exhibit a  
361 cosine variation consistent with the cosine dependence predicted by Eq. (2). A cosine  
362 function is fitted to the observations to estimate the radar beam pointing parameters.  
363 The amplitude of the fitted cosine function corresponds to a zenith pointing angle  $\theta_0$   
364 of approximately  $87.5^\circ$ , indicating an off-zenith pointing of about  $2.5^\circ$ . The phase shift  
365 provides an estimate of the azimuth pointing direction  $\phi_0$  of approximately  $140^\circ$ ,  
366 indicating the direction of beam tilt relative to geographic north.

#### 367 4.2 MWACR Observations from the CAPE-k

368 The same analysis procedure is applied to MWACR observations collected during the  
369 CAPE-k field campaign to evaluate beam pointing characteristics and provide an  
370 independent comparison with KAZR. Figure 6 summarizes the MWACR observations  
371 using data from the full campaign period. Figure 6b shows Doppler velocity as a  
372 function of wind direction. The MWACR Doppler velocity exhibits variability associated  
373 with changes in horizontal wind speed, superimposed on a mean Doppler velocity of  
374 approximately  $-0.7 \text{ m s}^{-1}$ , consistent with expected fall speeds of ice particles.  
375 Compared with KAZR, the MWACR Doppler velocity shows a smaller wind-direction-  
376 dependent modulation, indicating a weaker influence of horizontal wind projection.

377 Figure 6c shows the normalized Doppler velocity ( $V_d/U$ ) as a function of wind direction.  
378 After normalization by horizontal wind speed, the MWACR observations exhibit a  
379 relatively weak cosine dependence on wind direction compared with KAZR. The fitted  
380 cosine function yields a zenith pointing angle of approximately  $89.4^\circ$ , corresponding  
381 to an off-vertical pointing of about  $0.6^\circ$ . The fitted azimuth angle indicates the direction  
382 of the small residual beam tilt. The fitted constant offset of approximately  $-0.69 \text{ m s}^{-1}$   
383 represents the combined contribution of mean particle fall velocity and vertical air  
384 motion within the analyzed ice cloud layers.

385 The weaker cosine dependence of  $V_d/U$  on wind direction suggests that the MWACR  
386 beam is closer to vertical than the KAZR beam during this campaign period. Besides  
387 the beam width difference in radars, differences in the amplitude of the fitted cosine



388 relationship indicate that the stronger wind-direction dependence observed in KAZR  
389 Doppler velocity is likely associated with a larger beam pointing offset.

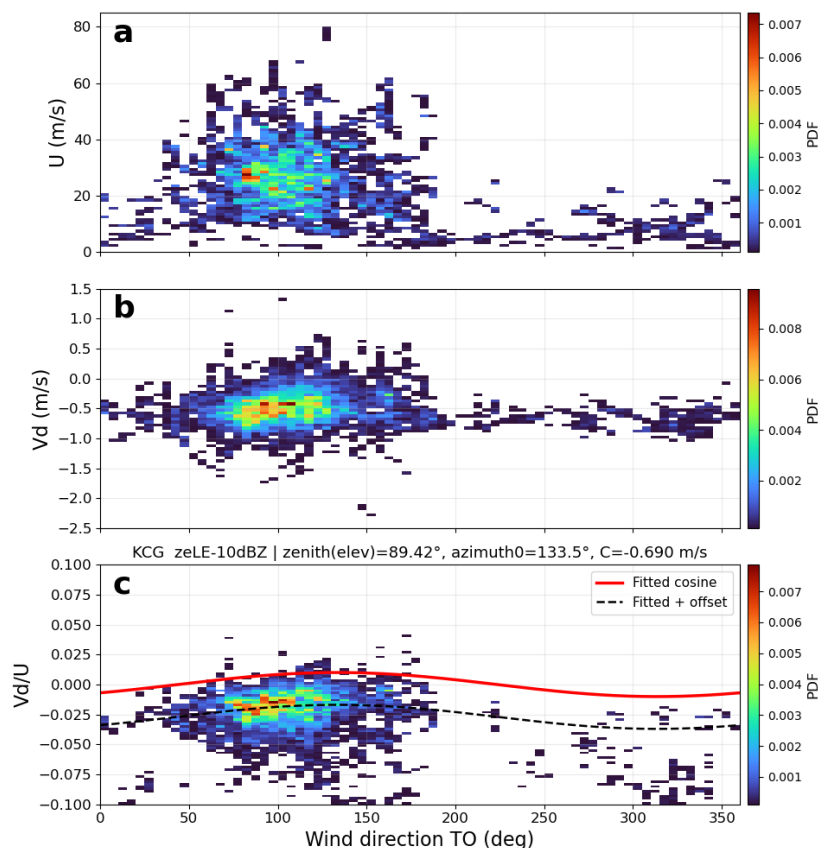


Figure 6. Same as Figure 5, but for MWACR at CAPE-k.

390

#### 391 4.3 Difference Between KAZR and MWACR Doppler Velocity

392 To further validate the beam-pointing estimation method, the Doppler velocity  
393 difference between KAZR and MWACR is examined. Because the two radars observe  
394 nearly the same atmospheric volume, the contributions from particle fall velocity ( $V_f$ )  
395 and vertical air motion ( $W$ ) are expected to be similar. Taking the Doppler velocity  
396 difference therefore reduces the influence of these atmospheric contributions and  
397 emphasizes differences associated with radar beam pointing.



398 The Doppler velocity difference is defined as

399 
$$\Delta v_d = v_{d,KAZR} - v_{d,MWACR}$$

400 Assuming that the contributions from particle fall velocity and vertical air motion largely  
401 cancel, the Doppler velocity difference can be approximated as

402 
$$\Delta v_d \approx U \cos(\phi - \phi_0) \cos(\theta_0) + C,$$

403 where  $U$  is horizontal wind speed,  $\phi$  is wind direction,  $\phi_0$  is the effective azimuth angle  
404 of the relative beam pointing offset,  $\theta_0$  is the effective zenith angle of the relative  
405 pointing offset, and  $C$  is a constant offset term. After normalization by horizontal wind  
406 speed,

407 
$$\frac{\Delta v_d}{U} \approx \cos(\phi - \phi_0) \cos(\theta_0) + \frac{C}{U}$$

408 For sufficiently strong winds, the second term becomes small, and the normalized  
409 Doppler velocity difference is approximately described by a cosine dependence on  
410 wind direction.

411 Figure 7 shows the Doppler velocity difference between KAZR and MWACR for all  
412 radiosonde cases during the field campaign. Panel (a) is identical to Figs. 5a and 6a.  
413 Panel (b) shows the Doppler velocity difference as a function of wind direction. The  
414 mean  $\Delta v_d$  is close to zero, indicating that the contributions from particle fall velocity  
415 and vertical air motion largely cancel, as expected. The Doppler velocity difference  
416 exhibits a systematic wind-direction dependence, with maximum values of  
417 approximately 1–1.5 m s<sup>-1</sup> occurring near a wind direction of about 140°.

418 Panel (c) shows the normalized Doppler velocity difference,  $\Delta v_d/U$ , as a function of  
419 wind direction. Compared with the individual radar results, the normalized difference  
420 exhibits a clearer cosine dependence and a much smaller constant offset. The fitted  
421 cosine relationship indicates an effective elevation angle of approximately 88.5°,  
422 corresponding to a relative off-vertical pointing of about 1.5°, and an azimuth direction  
423 near 140°. The near-zero offset term indicates that differencing largely removes the



424 mean contributions from particle fall velocity and vertical air motion that appear as  
425 offsets in the individual radar analyses.

426 This result provides an important validation of the method. Because the differencing  
427 approach suppresses the common atmospheric contributions to Doppler velocity, the  
428 remaining wind-direction-dependent signal more directly reflects the relative beam  
429 pointing difference between the two radars. The consistency between the individual-  
430 radar fits and the difference analysis supports the interpretation that the observed  
431 cosine dependence of Doppler velocity on wind direction primarily results from radar  
432 beam mispointing.

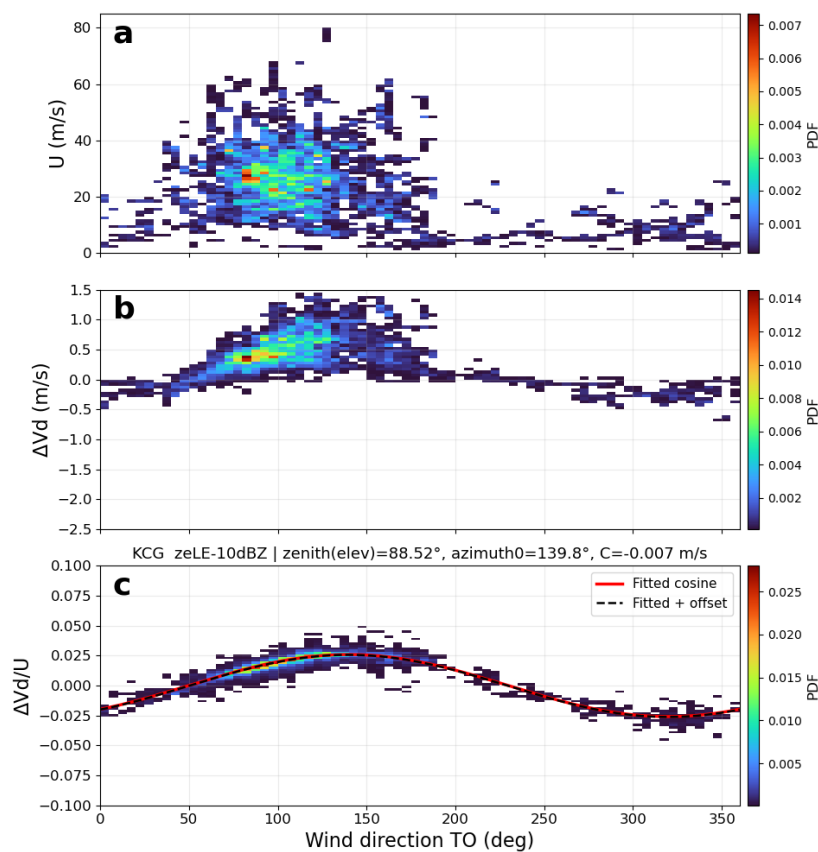


Figure 7 Same as Figures 5 and 6, but for the difference in Doppler velocity ( $\Delta Vd$ ) between KAZR and MWACR.

433



434 4.4 Application to the recent campaigns and fixed sites

435 To assess whether the proposed beam-pointing validation method is applicable  
436 beyond the CAPE-k campaign, the same analysis was applied to KAZR observations  
437 collected during the Bankhead National Forest (BNF, Kuang et al., 2026) and other field  
438 campaigns. As in the CAPE-k analysis, Doppler velocity observations were paired with  
439 collocated radiosonde wind profiles. Only data from ice cloud layers above the melting  
440 level were retained to reduce the influence of precipitation fall velocity. The normalized  
441 Doppler velocity,  $V_d/U$ , was then analyzed as a function of wind direction to identify  
442 the expected cosine dependence associated with radar beam pointing offsets.

443 Figure 8 summarizes the KAZR observations from the BNF campaign. Panel (a)  
444 shows horizontal wind speed as a function of wind direction derived from radiosonde  
445 measurements. Similar to CAPE-k, the BNF dataset includes a broad range of wind  
446 speeds, typically between 10 and 60  $\text{m s}^{-1}$ , with occasional stronger winds exceeding  
447 80  $\text{m s}^{-1}$ , providing sufficient variability for evaluating the wind-projection component  
448 of Doppler velocity. Panel (b) shows the corresponding KAZR Doppler velocity  
449 observations. The mean Doppler velocity is approximately  $-0.5 \text{ m s}^{-1}$ , consistent with  
450 expected fall speeds of ice particles. The wind-direction-dependent variability in  
451 Doppler velocity is weaker than that observed for KAZR at CAPE-k and is comparable  
452 in magnitude to the MWACR results shown in Fig. 6. Panel (c) shows the normalized  
453 Doppler velocity,  $V_d/U$ , as a function of wind direction. The normalized observations  
454 exhibit a weak but systematic cosine dependence consistent with the cosine  
455 relationship predicted for small beam pointing offsets.

456 The cosine fit shown in Fig. 8c yields a retrieved elevation angle of approximately  
457  $89.5^\circ$ , corresponding to an off-vertical pointing offset of about  $0.5^\circ$ , and an azimuth  
458 angle near  $130^\circ$ . The fitted constant offset is approximately  $-0.5 \text{ m s}^{-1}$ , reflecting  
459 residual contributions from mean particle fall velocity and vertical air motion.  
460 Compared with the CAPE-k KAZR result, the weaker cosine signal at BNF indicates a  
461 smaller beam pointing offset during this campaign period.

462 The estimated off-vertical pointing angle of about  $0.5^\circ$  is relatively small and is  
463 comparable to expected uncertainties associated with both instrument characteristics  
464 and the retrieval method. Several factors can contribute to this level of uncertainty.



465 First, the effective beam direction can be influenced by the radar beam width and  
466 sidelobe structure. Even if the radar container and antenna mount are mechanically  
467 aligned with the local vertical, slight asymmetries in the antenna radiation pattern or  
468 sidelobe contamination may introduce a small effective tilt in the zenith beam. Second,  
469 partial beam filling near cloud boundaries or horizontal inhomogeneity in ice cloud  
470 layers can introduce variability in the observed Doppler velocity that is not related to  
471 beam pointing. Third, spatial separation between the radar sampling volume and  
472 radiosonde wind measurements introduces representativeness uncertainty,  
473 particularly in environments with strong wind shear or horizontal variability.

474

475

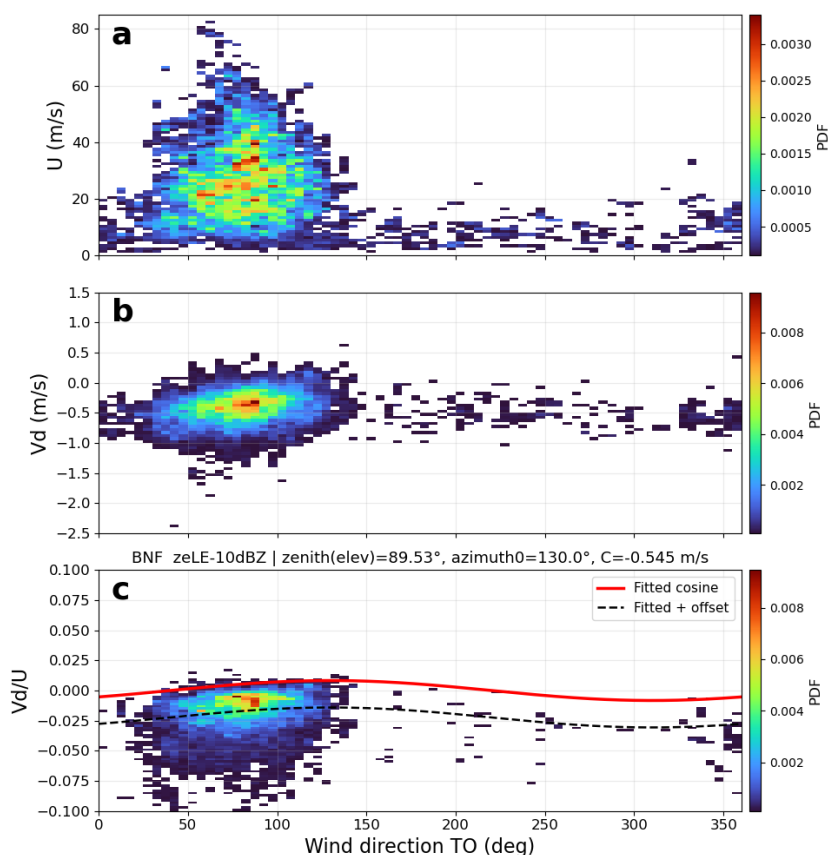


Figure 8. Same as Figure 5, but for KAZR at BNF



476 Additional uncertainty arises from methodological choices used in the Doppler velocity  
477 averaging and fitting procedure. Sensitivity tests using averaging windows of 30, 50,  
478 90, 120, and 150 minutes show that the retrieved elevation angle varies by less than  
479  $0.3^\circ$ . Sensitivity tests to particle fall velocity effects were performed by applying  
480 reflectivity thresholds of  $-30$ ,  $-20$ ,  $-10$ , and  $0$  dBZ to select ice cloud layers with  
481 different particle size characteristics. The fitted elevation angle varies by less than  $0.25^\circ$   
482 across these thresholds. Considering these factors together, the overall uncertainty in  
483 the estimated beam pointing angle is on the order of  $0.5^\circ$ .

484 These results indicate that the proposed method provides stable and physically  
485 consistent estimates of beam pointing across different field campaigns. The relatively  
486 small pointing offsets retrieved at BNF, together with the larger offset identified at  
487 CAPE-k, demonstrate that the method is capable of detecting both small and moderate  
488 deviations from vertical pointing while maintaining uncertainty within approximately  
489  $0.5^\circ$ .

490 The estimated beam-pointing offsets for recent ARM field campaigns, including the  
491 Surface Atmosphere Integrated Field Laboratory (SAIL), TRacking Aerosol  
492 Convection interactions ExpeRiment (TRACER), Eastern Pacific Cloud Aerosol  
493 Precipitation Experiment (EPCAPE), Coast-Urban-Rural Atmospheric Gradient  
494 Experiment (CoURAGE), CAPE-k, and BNF, are summarized in Table 1. Long-term  
495 results for the fixed ARM sites—the Southern Great Plains (SGP), North Slope of  
496 Alaska (NSA), and Eastern North Atlantic (ENA)—from 2011–2025 are presented in  
497 Figure 9. Overall, the retrieved pointing offsets for most field deployments are within  
498 approximately  $0.5^\circ$ , indicating generally good mechanical alignment of the radar  
499 antenna relative to the local vertical despite challenges associated with instrument  
500 transport, installation, and variable environmental conditions encountered during field  
501 operations. Two campaigns show larger deviations: CoURAGE exhibits a moderate  
502 offset ( $\sim 1.2^\circ$ ), while CAPE-k shows the largest offset ( $\sim 2.5^\circ$  for KAZR). These results  
503 demonstrate that most ARM field deployments maintain near-vertical pointing within  
504 the expected uncertainty range, and that the proposed method is sufficiently sensitive

505

506

507



Table 1. Estimated KAZR and MWACR Beam Pointing tilting from vertical for fixed sites and recent field campaigns.

	Site / Campaign	Time Period	Tilt from Vertical (°)
<b>Fixed Sites</b>	SGP	2011-2025	Figure 9
	NSA	2011-2025	Figure 9
	ENA	2016-2025	Figure 9
<b>Field Campaigns</b>	BNF (BNF)	2024-10-01-current	~0.5
	CoURAGE (CRG)	2024-12-01-2025-11-30	~1.2
	CAPE-k (KCG)	2024-04-15-2025-10-15	~2.5 (KAZR)
			~0.6 (MWACR)
	EPCAPE (EPC)	2023-02-15-2024-02-14	~0.3
	TRACER (HOU)	2021-10-01-2022-09-30	~0.1
SAIL (GUC)	2021-09-01-2023-06-15	~0.4	

508

509

510

511 to identify significant alignment deviations when they occur.

512 For the long-term fixed sites, the results indicate stable pointing performance at SGP  
 513 and NSA, with typical offsets near 0.5° throughout the 2011–2025 period. This  
 514 consistency reflects the effectiveness of routine maintenance and periodic instrument  
 515 levelling performed by ARM radar mentors. A notable deviation is observed at ENA  
 516 during 2017–2018, where the retrieved pointing offset increases relative to other  
 517 periods, which resulted increased Doppler velocity as reported by ARM data quality  
 518 report (<https://adc.arm.gov/ArchiveServices/DQRSservice?dgrid=D190321.8>). ARM  
 519 corrective maintenance (CM) records document a radar leveling procedure conducted  
 520 in January 2019, after which the estimated pointing offset decreased to approximately  
 521 0.1°, indicating restoration of near-vertical alignment. The improved pointing stability  
 522 following this maintenance activity highlights the importance of periodic mechanical



523 verification and adjustment of radar alignment, particularly after instrument relocation,  
524 exposure to severe environmental conditions, or extended operational periods.

525 Together, Table 1 and Figure 9 demonstrate that the proposed method can be applied  
526 consistently across both short-term field deployments and long-term operational sites,  
527 providing a unified and quantitative framework for evaluating radar pointing  
528 performance across the ARM KAZR network. The results also illustrate how beam  
529 pointing diagnostics can complement routine instrument maintenance records by  
530 identifying periods of potential misalignment and providing an independent  
531 observational constraint on radar mechanical stability.

532

533

534

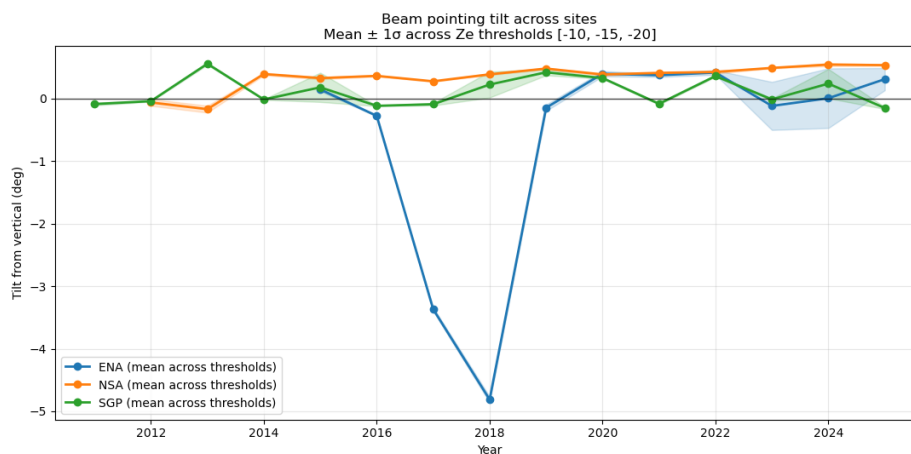


Figure 9. Time series of the mean KAZR beam-pointing tilt from vertical at the ENA, NSA, and SGP sites during 2011–2025. Tilt estimates are derived using multiple radar reflectivity ( $Z_e$ ) thresholds ( $-10$ ,  $-15$ , and  $-20$  dBZ) to filter the observations used in the pointing estimation. Shaded regions represent the standard deviation of the tilt estimates obtained using the different  $Z_e$  thresholds, indicating the sensitivity of the retrieval to reflectivity-based data selection. The results show generally stable pointing within approximately  $0.5^\circ$  at NSA and SGP over the analysis period, while a larger deviation is evident at ENA during 2017–2018.



## 535 **5 Summary**

536 Accurate beam pointing is essential for vertically pointing cloud radars because  
537 Doppler velocity measurements are widely used to infer vertical air motion and  
538 hydrometeor fall velocity. Even small deviations from vertical pointing introduce a  
539 horizontal wind contribution through geometric projection onto the radar beam,  
540 potentially biasing the interpretation of cloud dynamical and microphysical processes.  
541 In this study, we developed and evaluated a method to estimate and validate beam  
542 pointing offsets of vertically pointing cloud radars using collocated radiosonde wind  
543 measurements.

544 The method is based on the cosine dependence of Doppler velocity on horizontal wind  
545 direction when the radar beam deviates slightly from the vertical direction. By  
546 normalizing Doppler velocity by horizontal wind speed, the dependence on wind  
547 magnitude is reduced and the remaining variability primarily reflects radar beam  
548 pointing geometry. The normalized Doppler velocity ( $V_d/U$ ) exhibits a cosine variation  
549 with wind direction, allowing quantitative estimation of radar zenith and azimuth  
550 pointing offsets through cosine fitting. Sensitivity tests indicate that the uncertainty in  
551 the retrieved pointing angle is on the order of  $0.5^\circ$ , demonstrating that the method can  
552 detect both small and moderate deviations from vertical pointing.

553 Application of the method to observations from the CAPE-k field campaign shows  
554 detectable pointing offsets for both KAZR and MWACR, with KAZR exhibiting a larger  
555 off-vertical deviation than MWACR during this period. Analysis of the Doppler velocity  
556 difference between the two radars reduces the influence of particle fall velocity and  
557 vertical air motion, resulting in a clearer wind-direction-dependent signal and providing  
558 an independent constraint on relative beam pointing differences.

559 The method was also applied to observations from the BNF field campaign to evaluate  
560 its applicability under different atmospheric conditions. Results from BNF indicate very  
561 small off-vertical pointing offsets, demonstrating consistency with expected radar  
562 alignment and confirming the stability of the retrieval approach. The successful  
563 application of the method across multiple field campaigns demonstrates its robustness  
564 and general applicability.



565 Overall, small beam pointing offsets produce measurable Doppler velocity signals  
566 through projection of horizontal wind onto the radar beam. Normalization using  $V_d/U$   
567 isolates radar beam pointing geometry from variability in wind magnitude. Cosine  
568 fitting of the wind-direction dependence provides quantitative estimates of radar zenith  
569 and azimuth pointing angles. Differencing Doppler velocity between co-located radars  
570 reduces uncertainty associated with particle fall velocity and vertical air motion. The  
571 method is applicable across multiple field campaigns and atmospheric conditions.

572 Because radiosonde observations are routinely available at many atmospheric  
573 measurement sites, the proposed method provides a practical and independent  
574 approach for monitoring and validating beam pointing of vertically pointing cloud  
575 radars. The approach can improve interpretation of Doppler velocity observations and  
576 support long-term consistency of radar-derived cloud and vertical velocity products.

577

578 Data availability

579

580 The Atmospheric Radiation Measurement Climate Research Facility KAZR and  
581 MWACR data used in this study, including observations from the CAPE-k, BNF,  
582 CoURAGE, EPCAPE, SAIL, and TRACER campaigns, as well as the fixed ARM sites  
583 SGP, ENA, and NSA, are available as ARM a1-level data products. The radiosonde  
584 data are obtained from the calibrated ARM sondewnpn.b1 datastream, and all  
585 datasets are publicly accessible through the ARM Data Discovery portal at ARM Data  
586 Discovery.

587 The beam-pointing estimation algorithm has been implemented at the ARM Data  
588 Quality Office for long-term monitoring applications. The code is available from the  
589 lead author, Dr. Min Deng, upon request via email ([mdeng@bnl.gov](mailto:mdeng@bnl.gov)).

590

591

592



593 Acknowledgement

594

595 Contributions from Brookhaven National Laboratory co-authors were supported by the  
596 Atmospheric Radiation Measurement (ARM) Facility and the Atmospheric System  
597 Research (ASR) program of the Office of Biological and Environmental Research in  
598 the U. S. Department of Energy, Office of Science, through Contract No. DE-  
599 SC0012704. Pacific Northwest National Laboratory (PNNL) is operated by Battelle for  
600 the U. S. Department of Energ. The authors from PNNL are also supported by ARM  
601 through Contract No. DE-SC0015990.

602

603 **References**

604 Dirksen, R. J., Sommer, M., Immler, F., Hurst, D. F., Kivi, R., and Vömel, H.: Reference  
605 quality upper-air measurements: GRUAN data processing for the Vaisala RS92  
606 radiosonde, *Atmos. Meas. Tech.*, 7, 4463–4490, [https://doi.org/10.5194/amt-7-](https://doi.org/10.5194/amt-7-4463-2014)  
607 [4463-2014](https://doi.org/10.5194/amt-7-4463-2014), 2014.

608 Deng, M., and G. G. Mace, 2006: Cirrus Microphysical Properties and Air Motion  
609 Statistics Using Cloud Radar Doppler Moments. Part I: Algorithm Description. *J.*  
610 *Appl. Meteor. Climatol.*, 45, 1690–1709, <https://doi.org/10.1175/JAM2433.1>.

611 Deng, M., and G. G. Mace, 2008: Cirrus microphysics properties and air motion  
612 statistics using MMCR Doppler moments: Water content, particle size and  
613 sedimentation relationships. *GRL*, 35, L17808, doi:10.1029/2008GL035054 (13)

614 Doviak, R. J. and Zrnić, D. S.: *Doppler Radar and Weather Observations*, Academic  
615 Press, San Diego, USA, 1993.

616 Kalesse, H., and P. Kollias, 2013: Climatology of high cloud dynamics using profiling  
617 ARM Doppler radar observations. *J. Climate*, 26, 6340–6359,  
618 doi:10.1175/JCLI-D-12-00695.1.

619 Keeler, E. *Balloon-Borne Sounding System (SONDE) Instrument Handbook*. U.S.  
620 Department of Energy, Atmospheric Radiation Measurement user facility,  
621 Richland, Washington. DOE/SC-ARM-TR029.



- 622 Kollias, P., Albrecht, B. A., and Marks, F.: Why Mie? Accurate observations of vertical  
623 air velocities and raindrops using a cloud radar, *Bull. Amer. Meteor. Soc.*, 83,  
624 1471–1483, <https://doi.org/10.1175/BAMS-83-10-1471>, 2002.
- 625 Kollias, P., Bharadwaj, N., Widener, K., Jo, I., and Johnson, K.: Scanning ARM cloud  
626 radars. Part I: Operational sampling strategies, *J. Atmos. Ocean. Technol.*, 31,  
627 569–582, <https://doi.org/10.1175/JTECH-D-13-00044.1>, 2014.
- 628 Kollias, P., and Coauthors, 2016: Development and Applications of ARM Millimeter-  
629 Wavelength Cloud Radars. *Meteor. Monogr.*, 57, 17.1–  
630 17.19, <https://doi.org/10.1175/AMSMONOGRAPHS-D-15-0037.1>.
- 631 Kollias, P., Clothiaux, E. E., Albrecht, B. A., Miller, M. A., Moran, K. P., and Johnson,  
632 K. L.: The Atmospheric Radiation Measurement Program cloud profiling radars:  
633 Second-generation sampling strategies, processing, and cloud data products,  
634 *J. Atmos. Ocean. Technol.*, 24, 1199–1214,  
635 <https://doi.org/10.1175/JTECH2033.1>, 2007.
- 636 Kollias, P., Szyrmer, W., Luke, E., & McFarquhar, G. (2007).  
637 On the estimation of vertical air motion using cloud radar Doppler spectra.  
638 *Journal of Atmospheric and Oceanic Technology*, 24, 1805–1821.  
639 <https://doi.org/10.1175/JTECH2081.1>
- 640 Kollias, P., Szyrmer, W., Luke, E., & McFarquhar, G. (2007).  
641 On the estimation of vertical air motion using cloud radar Doppler spectra.  
642 *Journal of Atmospheric and Oceanic Technology*, 24, 1805–1821.  
643 <https://doi.org/10.1175/JTECH2081.1>
- 644 Kuang, C., and Coauthors, 2026: The U.S. DOE ARM User Facility Establishes a New  
645 Site for Studies of Land–Aerosol–Cloud Interactions in the Southeastern United  
646 States. *Bull. Amer. Meteor. Soc.*, 107, E1–E8, [https://doi.org/10.1175/BAMS-](https://doi.org/10.1175/BAMS-D-25-0072.1)  
647 [D-25-0072.1](https://doi.org/10.1175/BAMS-D-25-0072.1).
- 648 Luke, E. P. and Kollias, P.: Separating cloud and drizzle radar moments during  
649 precipitation onset using Doppler spectra, *J. Atmos. Ocean. Technol.*, 30,  
650 1656–1671, <https://doi.org/10.1175/JTECH-D-11-00195.1>, 2013.



- 651 Mather, J. H. and Voyles, J. W.: The ARM Climate Research Facility: A review of  
652 structure and capabilities, *Bull. Amer. Meteor. Soc.*, 94, 377–392,  
653 <https://doi.org/10.1175/BAMS-D-11-00218.1>, 2013.
- 654 Moran, K. P., Martner, B. E., Post, M. J., Kropfli, R. A., Welsh, D. C., and Widener, K.  
655 B.: An unattended cloud-profiling radar for use in climate research, *Bull. Amer.*  
656 *Meteor. Soc.*, 79, 443–455, [https://doi.org/10.1175/1520-](https://doi.org/10.1175/1520-0477(1998)079<0443:AUCPRF>2.0.CO;2)  
657 [0477\(1998\)079<0443:AUCPRF>2.0.CO;2](https://doi.org/10.1175/1520-0477(1998)079<0443:AUCPRF>2.0.CO;2), 1998.
- 658 Nash, J., Oakley, T., Vömel, H., and Wei, L.: WMO intercomparison of high quality  
659 radiosonde systems, WMO Instruments and Observing Methods Report No.  
660 107, World Meteorological Organization, Geneva, Switzerland, 2011.
- 661 Shupe, M. D., Kollias, P., Matrosov, S. Y., and Schneider, T. L.: Deriving mixed-phase  
662 cloud properties from Doppler radar spectra, *J. Atmos. Ocean. Technol.*, 21,  
663 660–670, [https://doi.org/10.1175/1520-](https://doi.org/10.1175/1520-0426(2004)021<0660:DMCPFD>2.0.CO;2)  
664 [0426\(2004\)021<0660:DMCPFD>2.0.CO;2](https://doi.org/10.1175/1520-0426(2004)021<0660:DMCPFD>2.0.CO;2), 2004.
- 665 Shupe, M. D., J. M. Comstock, D. D. Turner, and G. G. Mace, 2016: Cloud Property  
666 Retrievals in the ARM Program. *Meteor. Monogr.*, 57, 19.1–  
667 19.20, <https://doi.org/10.1175/AMSMONOGRAPHS-D-15-0030.1>.
- 668 Shupe, M. D., Kollias, P., Poellot, M., and Eloranta, E.: A focus on mixed-phase clouds:  
669 The status of ground-based observational methods, *Bull. Amer. Meteor. Soc.*,  
670 89, 1549–1562, <https://doi.org/10.1175/2008BAMS2378.1>, 2008.
- 671 Shupe, M. D., Kollias, P., Poellot, M., & Eloranta, E. (2008).  
672 On deriving vertical air motions from cloud radar Doppler spectra in mixed-  
673 phase Arctic clouds. *Journal of Atmospheric and Oceanic Technology*, 25, 547–557.  
674 <https://doi.org/10.1175/2007JTECHA1007.1>
- 676 Zhu, Z., Kollias, P., Yang, F., & Luke, E. (2021).  
677 On the estimation of in-cloud vertical air motion using radar Doppler spectra.  
678 *Geophysical Research Letters*, 48, e2020GL090682.  
679 <https://doi.org/10.1029/2020GL090682>
- 680 Zhu, Z., Kollias, P., & Yang, F. (2023).  
681 Particle inertial effects on radar Doppler spectra simulation.

<https://doi.org/10.5194/egusphere-2026-3304>

Preprint. Discussion started: 12 June 2026

© Author(s) 2026. CC BY 4.0 License.



682 Atmospheric Measurement Techniques, 16, 3727–3737.  
683 <https://doi.org/10.5194/amt-16-3727-2023>